Damage micromechanisms in dual-phase steel investigated by combined phase- and absorption-contrast tomography

In general, the ductile fracture process in alloys consists of the nucleation, growth and coalescence of microvoids. The nucleation of microvoids is attributable to particle fracture and/or particle/matrix interfacial decohesion. The ductile fracture process might also be interrelated with various microstructural heterogeneities, such as pre-existing microdefects [1], particle clustering [2], microstructural anisotropy [3] and dual-phase (DP) microstructures [4]. It is reasonable to assume that the ductile fracture process is appreciably affected in the case of a DP microstructure, which is seen in DP steels that consist of a hard martensitic phase and a soft ferritic phase. In spite of extensive research activity, a variety of interpretations remain concerning the micromechanisms of damage nucleation in DP steels. With the advent of state-of-the-art imaging techniques, a thorough understanding of the detailed damage processes is expected, even when practical materials with three-dimensional (3D) complexity in their DP microstructures are investigated. Phase-contrast X-ray microtomography (XMT) techniques are capable of revealing such DP microstructures with reasonable spatial resolution. The present authors applied the single-distance phase retrieval technique to 3D observations of a DP stainless steel consisting of austenitic and ferritic phases [5,6], In the present study, the single-distance phase retrieval technique was applied to contrast-enhanced imaging of the DP microstructure of a ferrite/martensite DP with only 1.4% difference in density between the two phases [7]. The XMT experiments were performed at SPring-8 **BL20XU** beamline.

The loading step at which each microvoid was nucleated was identified by tracking the microvoid throughout the application of tension, together with its nucleation site. The growth curves of individual microvoids are collated and classified according to their nucleation site in Fig. 1. Wider variation in the growth rate is apparent in the case of microvoids nucleated due to martensitic cracking. The four microvoids with high growth rates were nucleated by martensitic cracking at an applied strain of 23.9%, and later propagated in oblique directions with respect to the loading direction.

The largest microvoid seen in Fig. 1 has been extracted in Fig. 2, together with adjacent martensitic particles. The microvoids shown in Fig. 2 were nucleated where the martensitic phase exhibited morphological complexity such as a notch or neck.

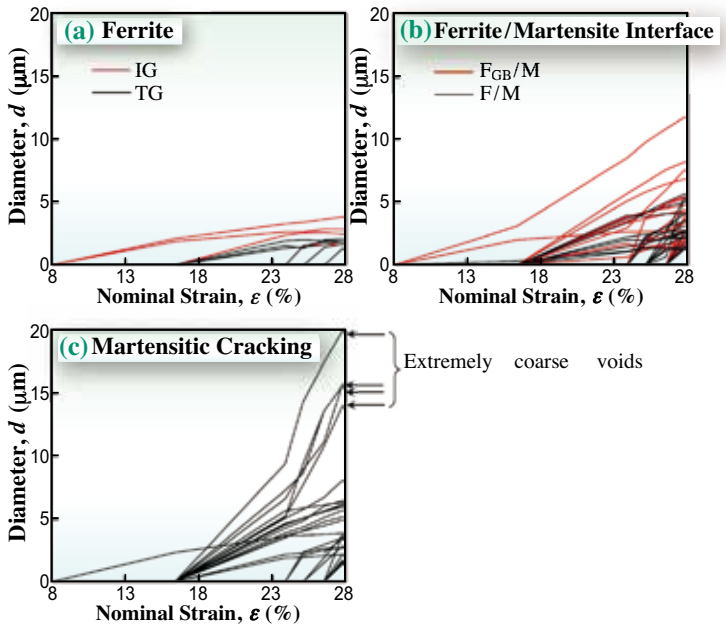

Fig. 1. Growth behavior of individual microvoids extracted from a unit box located at the center of the specimen. The growth data were organized according to the microvoid nucleation sites: **(a)** microvoids nucleated in the ferritic phase, which have been classified into intergranular (IG) and transgranular (TG) fracture; **(b)** the interfaces between the ferritic and martensitic phases, in which the intersections between martensite and the ferritic grain boundaries have been distinguished; and **(c)** the martensite fracture itself.

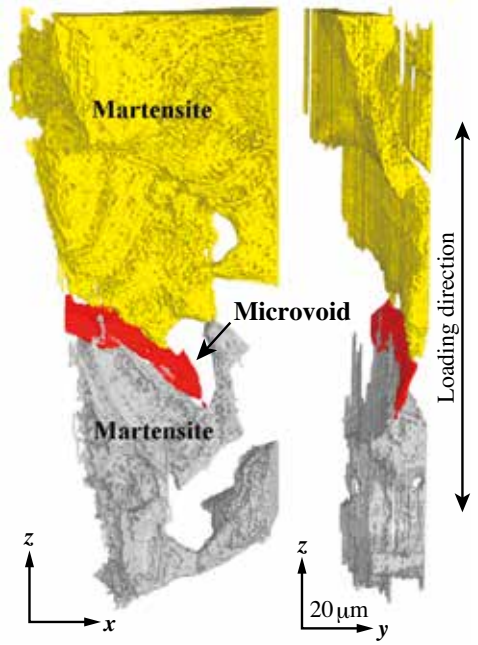

Fig. 2. 3D perspective views of a typical microvoid. The underlying ferritic phase is not displayed, and only the microvoid and the martensitic phase are shown.

No such morphological features were obvious at the other nucleation sites. It is clearly demonstrated that necked portions were sampled as a result of intense strain localization, and that the driving forces for subsequent rapid growth may arise from stress redistribution after martensitic cracking. In order to quantitatively evaluate the effects of the martensitic morphology, 3D strain mapping was performed for the interior of the martensitic phase. Tetrahedra, whose vertices were sites of morphological features such as concave and convex portions of the martensitic phase, were generated by the Delaunay tessellation technique, and normal and shear strains were then calculated on the basis of the deformation of each tetrahedron, assuming a linear displacement field inside it. The local strain distribution was illustrated in the form of a 3D color contour map, as shown in Fig. 3. It is interesting to note that in this figure, although the macroscopic applied strain range is only 11.4% (i.e., between the third and the last loading steps), high strain regions reach more than 50% in terms of the equivalent strain shown in Fig. 3(b).

Premature damage initiation was observed at a relatively early stage at various nucleation sites, such as the ferrite interior, martensitic interior and ferrite/martensite interfaces; however, the subsequent growth of such microvoids was relatively moderate. On the other hand, microvoids were also initiated later by martensitic cracking after the maximum load was reached, and these microvoids subsequently exhibited rapid growth. The martensite cracking induced additional damage evolution, mainly along nearby ferrite/martensite interfaces and intersections between the martensite and the ferrite grain boundaries. It is notable that the microvoids originating from martensitic cracking exhibited characteristic shear-dominated growth under macroscopic tension, whereas those originating from the other nucleation sites exhibited traditional triaxiality-dominated growth. It was concluded that the ductile fracture was dominated by the substantial force driving the growth of microvoids located on morphologically characteristic martensitic particles.

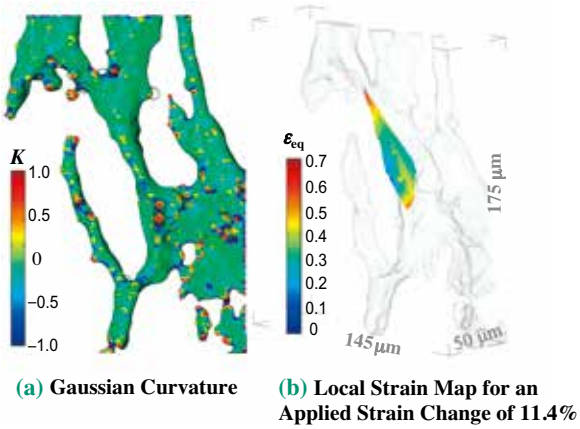

(a) Gaussian Curvature **(b) Local Strain Map for an Applied Strain Change of 11.4%**

Fig. 3. Results of 3D strain mapping of cracked martensite, which was measured between an applied strain of 16.4 and 27.8%. **(a)** Spatial distribution of Gaussian curvature value superposed on the extracted image of a martensitic phase region. **(b)** 3D contour of equivalent strain. Circles in **(a)** denote morphological features used for the 3D strain mapping.

Kyosuke Hirayama[a,*], Hiroyuki Toda[a] and Masakazu Kobayashi[b]

[a] Department of Mechanical Engineering, Kyushu University
[b] Department of Mechanical Engineering, Toyohashi University of Technology

*Email: hirayama@mech.kyushu-u.ac.jp

References

[1] H. Toda *et al.*: Metall. Mater. Trans. A **45** (2014) 765e776; L. Margulies *et al.*: Science **291** (2001) 2392.
[2] D. Steglich *et al.*: Eng. Fract. Mech. **75** (2008) 3692.
[3] C.Y. Tang *et al.*: J. Mater. Proc. Tech. **91** (1999) 270.
[4] E. Ahmad *et al.*: J. Mater. Eng. Perform. **21** (2012) 382.
[5] H. Toda *et al.*: ISIJ Int. **56** (2016) 883.
[6] H. Toda *et al.*: Proc. 4th Int. Symposium Steel Sci. (2014) 32.
[7] *H. Toda, A. Takijiri, M. Azuma, S. Yabu, K. Hayashi, D. Seo, M. Kobayashi, K. Hirayama, A. Takeuchi, K. Uesugi: Acta Materialia* ***126*** *(2017) 401.*